Retinal Plasticity: Functional Recovery after Bipolar Cell Loss in the Oxygen Induced Retinopathy Model

BioRxiv submission Version 12-12-2019

K.P. Mitton[1], M. Deshpande[1], S.C. Wong[1,3], E. Guzman[1], M. Cheng[1], W. Dailey[1], R. Schunemann[1,4], M. Trese[1,2], K. Drenser[1,2]

1 Eye Research Institute - Pediatric Retinal Research Lab, Oakland University, Rochester, MI
2 Associated Retinal Consultants, Novi, MI.
3 Currently, Moorsfields Eye Hospital, Great Ormond Street Hospital for Children, and Royal Free Hospital, London, United Kingdom
4 Currently, Oftalmologica, Joinville, Santa Catarina, Brazil

Corresponding authors: Ken Mitton, mitton@oakland.edu, 248-370-2079. Kimberly Drenser kdrenser@arcpc.net

ABSTRACT

Purpose: Bipolar cells can perish during inner retinal ischemia resulting from disruption of the inner retinal microvasculature. Can surviving inner retinal neurons recover and integrate into the functional network after ischemic damage? Using the mouse oxygen induced retinopathy (OIR) model, we applied focal-ERG to determine if B-wave recovery occurs after ischemic bipolar cell death after revascularization.

Methods: The OIR model was used to generate regions of inner retinal neuron loss in B6.Cg-Tg$^{Thy1\text{-}YFP}$ mice. Using image-guided focal-ERG, the dark-adapted mixed rod-cone light response was compared using stimulation of small circular (0.27 mm diameter) target areas located in the central retinas of the same eyes (OIR and control). The same areas of the same retinas were followed over three ages after revascularization (P21, P28 and P42).

Results: There was a minimal effect on the photoreceptor-derived A-wave amplitude in the central damaged regions. B-wave amplitudes were almost absent in these damaged central regions at age P21, and progressively recovered through ages P28 to P42. The magnitude of the recovered B-wave amplitude by P42 remained less than the normal control retina (room air), but did show oscillatory potentials.

Conclusions: Recovery of retinal functionality, a neural plasticity, was detected in the central damaged regions of the mouse OIR model after the initial loss of bipolar cells and revascularization of these zones. These results suggest that any treatments that would enhance the overall survival of inner retinal neurons result in a significant improvement in neural function after any surviving neurons establish connectivity.

INTRODUCTION

While the Human retina is routinely monitored with non-invasive methods, there is a growing awareness that combining multiple imaging modes and targeted functional testing can provide a more complete understanding of both development and regional pathophysiology. In various Human retinal diseases, the initial pathology and the progress of retinal changes are rarely uniform throughout the entire retina area. There are often profound differences in both the radial direction and distance from the disc, or between the central and peripheral retina. Useful disease research models, such as the oxygen induced retinopathy (OIR) model, or testing of sub-retinal injections (genes/cells) would also benefit from the ability to compare different retinal areas within the same eye [1-4]. In this report, we describe the application of non-invasive retinal imaging, combined with focal-ERG, to explore the plasticity of the inner neural retina subsequent to the loss of inner retinal neurons, bipolar cells, after ischemia in the mouse OIR model.

In humans, damage to the post-photoreceptor sensitivity is common in retinopathy of prematurity (ROP) patients depending on the severity of disease (Fulton et al, 2009)[5]. Both photoreceptor sensitivity and post-photoreceptor response are diminished more in severe ROP compared to mild ROP patients, with cone responses less affected than rod responses (Fulton 2008)[6]. Rod photoreceptor function and post-photoreceptor function is also diminished in rat OIR models (Akula et al 2007) [7] (Fulton, Akula et al 2009) [8] More recent studies in humans indicate that some ROP patients likely experience recovery of post-photoreceptor function. This is based on the finding that older patients who were classified as having mild ROP as infants have improved post-photoreceptor function compared to infant mild ROP patients (Harris et al., 2011)[9]. Nakamura et al. (2012) reported an average reduction in the full-field ERG B-wave amplitude from the retinas of OIR mice, consistent with a significant loss of bipolar cells [10]. They also noted a partial recovery of the B-wave amplitude over several weeks post-damage.

Neural retinal maturation and retinal vascular development occurs post-natal in mice. For the oxygen induced retinopathy model, mice are exposed to 75% oxygen for five days, from age P7 to P12. This period starts about the time that the superficial vascular bed is just

reaching the peripheral retina, having originated from the optic disc. In the high oxygen environment the normal development of all three vascular beds is impaired and the superficial capillary bed degenerates through apoptosis. After five days of 75% oxygen, by age P12, the central retina is devoid of any capillary beds and thus avascular. Down-regulation of retinal *Vegf* (Vascular Endothelial Growth Factor) gene expression is a major factor responsible for this vaso-obliteration mechanism [11]. Upon return to room air (21% oxygen), this central retinal zone becomes hypoxic and that results in an increased concentration of VEGFA (vascular endothelial growth factor A) and an aggressive revascularization of the central retina [12]. This process brings oxygen back to the central retina by age P21. Until this recovery to normoxia by age P21, bipolar cell loss can be extensive in the central retina and the thinning of the INL (inner nuclear layer) may be substantial [13].

Since full-field ERG stimulates both the more central OIR damaged retina and the non-damaged peripheral retina, some questions remain regarding the nature of the B-wave recovery seen in both rat and mouse OIR models. Does post-photoreceptor function recover in the central damaged zones, or is the recovery of the full-field ERG B-wave simply originating in the otherwise undamaged peripheral retina? Upon initial OIR damage, are there regions with little or no post-photoreceptor B-wave response that still have substantial photoreceptor A-wave response? To answer these questions we employed a novel focal-ERG system to evaluate the relative function within the central zones of the OIR damaged retina over several weeks after revascularization.

METHODS

Animals - This study was approved by the Oakland University IACUC and complied with the ARVO Statement for the Use of Animals in Ophthalmic and Vision Research. Mice expressing YFP (yellow fluorescent protein) in a subset of ganglion cells (B6.Cg-Tg(Thy1-YFP)HJrs/J) were obtained from the Jackson Laboratory (Bar Harbor, ME).

104 *Oxygen-induced Retinopathy*- Pre-weanling litters were housed in 75% oxygen for five
105 days, as per Smith et al. (1993), from post-natal age P7 to P12. Litters were then returned to
106 room air. This exposure window was late enough to minimize dilation effects on the
107 regressing hyaloid vessels, and early enough to overlap with retinal vascular development.
108 A maximal neovascularization response occurs in this model between age P17 and P21.
109
110 *Micron-III system imaging and Focal-ERG* – Focal-ERG analysis was completed in the
111 Pediatric Retinal Research Laboratory's retinal imaging and ERG suite, at the Eye Research
112 Institute of Oakland University. The suite was equipped with variable dim red lighting (4-15
113 Lux) for working on dark-adapted rodents. Focal-ERG recordings were from dark-adapted
114 mice using a Micron-III camera-mounted focal-ERG system (Phoenix Research Labs,
115 Pleasanton CA). See **Figure 1**. After 1.5-hours of dark adaption in the suite's dark housing
116 station, pupils of mice were dilated with sequential application of tropicamide and
117 phenylephrine eye drops. To achieve a brief anesthesia (30 minutes), mice received a single
118 injection (IP) of 50 mg/kg Ketamine HCl and 7 mg/kg Xylazine. After loss of the blinking
119 reflex, eyes were protected by Goniovisc corneal protectant gel solution. This solution
120 provided optical coupling to the lens of the focal ERG attachment, and provided low
121 impedance for electrical coupling to a gold-plated lens-mount, which served as the
122 measuring electrode.

Figure 1. Micron-III System, Pediatric Retinal Research Lab, Eye Research Institute, Oakland University.
A) Focal ERG work-station. **B)** Micron-II camera with focal-ERG attachment and electrode interface. **C)** Focal-ERG attachment illumination targeting controls. **D)** Mouse warming support.

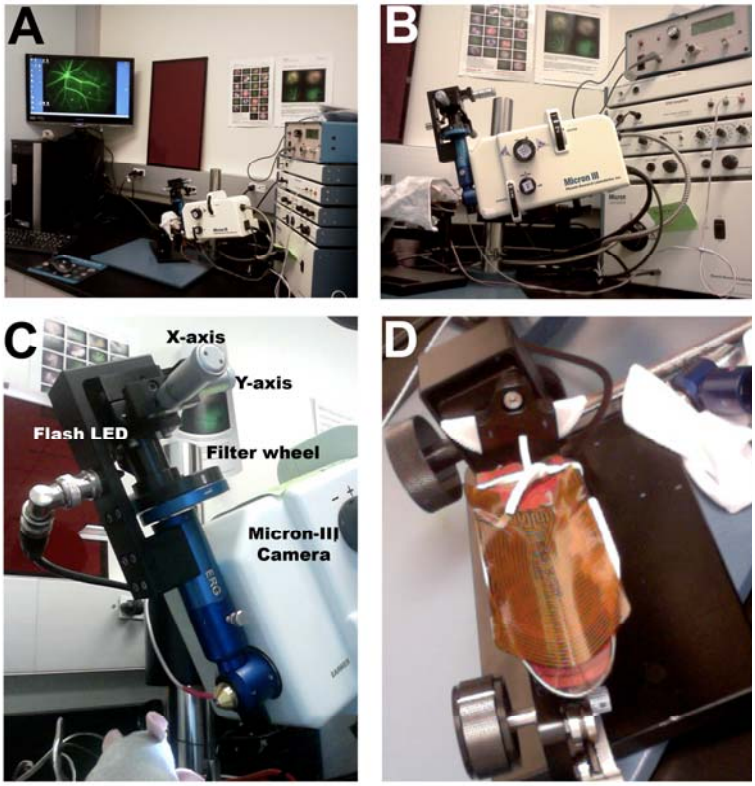

The mouse support included a thermal heating pad set for 37°C, which was necessary to avoid temperature loss under anesthesia. Aiming of the light stimulus was accomplished by viewing the retina with dim red-filtered LED illumination, high camera gain, and a 15-frame video averaging. (Otherwise not visible to the naked eye.) A small circular LED white-light stimulus just larger than the optic disc was projected to stimulate four positions around and adjacent to the optic disc (30 msec duration) with a bright intensity setting corresponded to an energy delivery of 43,775 cd-sec/m^2 of projected retinal area, sufficient to elicit a maximum mixed cone-rod response. The stimulus spot diameter was 0.27 mm, area 0.057 mm^2. The Micron-III focal-ERG had a high luminous efficiency cool-white LZ1-00CW00 LED (LED Engin, San Jose, CA) with emission from 430-650 nm. Platinum cutaneous needle-electrodes were used for the reference and ground, inserted into head-cap and hind-flank skin respectively. Triggering of the light stimulus and acquisition of the ERG traces were accomplished with LabScribe2 software equipped with the Phoenix Research Lab ERG module. Twenty stimulus traces were averaged to obtain the ERG trace, with a 100 msec delay between acquisition cycles. Band pass was set to range from 0.5 Hz to 2000 Hz and digitization rate was 5000 Hz.

Focal-ERG data were collected by targeting the same central retinal locations of the same eyes at three different ages: P21, P28 and P42. **Figure 2** illustrates the initial identification of the disc in an eye (left eye). The same spot was then decreased in size, in this case a spot size selection was fixed to a diameter of 0.27 mm , which was just larger than the optic disc itself (**Figure 2B**). This target size was used in continuous red-light mode to visualize placement into the desired target region, relative to the disc. Just prior to acquisition, the focal-ERG system was switched to flash illumination mode and the red filter removed for full white LED stimulation. Then ERG recordings were obtained in regions around the disc in the order: temporal, nasal, superior and inferior to the disc.

Fig 2. Focal-ERG Targeting Process of the dark-adapted retina. Images shown were obtained during acquisition of the P42 Oxygen-treated focal-ERG data shown in Figure-5. A) Dim red-light illumination, not visible to the naked eye, was used to visualize the optic disc by with high camera gain and 15-frame high-speed image summation. B) The illumination spot size was then reduced for targeting a circular area of 0.06 mm^2, just larger than the disc itself. For illustration purposes, the disc location is marked with a white cross. C) An example of targeting nasal to the disc, left eye. D) Example, targeting superior to the disc, same eye.

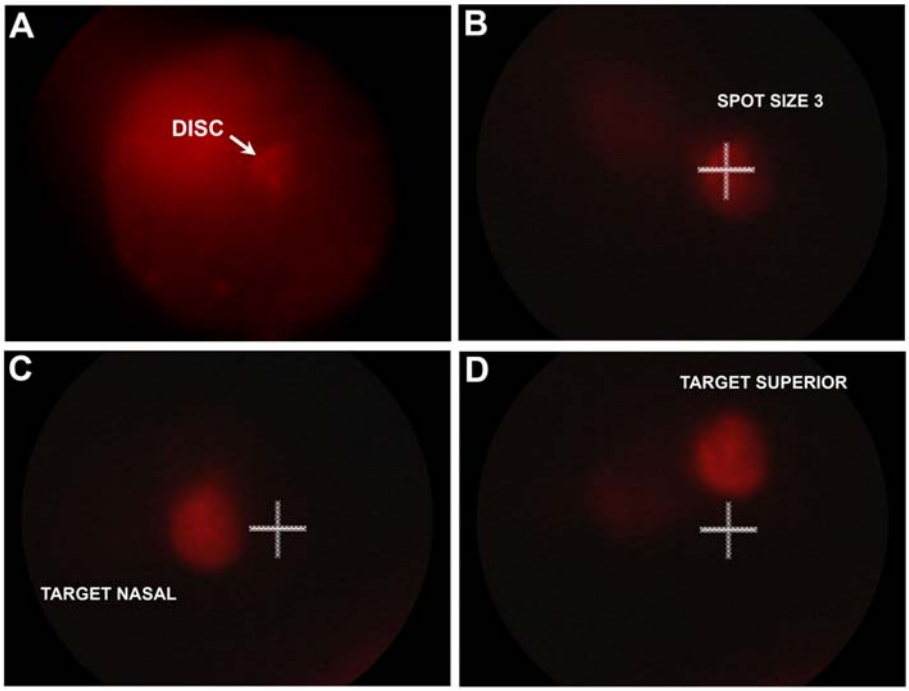

By using this targeting scheme, the same central regions (damaged by OIR), could be re-tested, longitudinally, in the same retinas following recovery at ages P21, P28 and P42. A-wave and B-wave amplitudes from the four locations in the retina were averaged at each age compared between normal and control retinas by t-test.

Spectral Domain Optical Coherence Tomography Analysis (SDOCT)- Linear B-scans were obtained using the SD-OCT injector attachment, for the mouse eye, mounted to a Micron-III Camera System (Phoenix Research Labs, CA). Pupils of mice were dilated with sequential application of tropicamide and phenylephrine eye drops. To achieve anesthesia (30 minutes), mice received a single injection (IP) of 50 mg/kg Ketamine HCl and 7 mg/kg Xylazine. Mice received a 50uL inujection (IP) of 10mg/mL fluorescein (in saline) to enable visualization of the retinal vasculature using a fluorescein filter set on the Micron-III imaging system. Eyes were kept wet using artificial tears. The linear b-scans were targeted during real time viewing of the retinal vasculature.

Virtual Microscopy for Morphology Analysis: Enucleated whole eyes were fixed in Davison's fixative. Fixed tissues were processed for paraffin sections and stained with hematoxylin & eosin. Sections were obtained near the optic nerve region to obtain full cross-sections of retina (7 µm thick) from periphery to periphery. Whole slides were digitized using a 20x objective lens and an Olympus SL120 Virtual Microscopy Slide Scanner, and saved in the vsi-file format. Digital files were managed and analyzed using Leica (Slidepath) Digital Image Hub and Digital Slide Box (DSB) web servers, with the Safari web browser (Apple, Cupertino, CA).

RESULTS

Loss of inner retinal neurons in the central retina of OIR mice.

Examples of retinal morphology are shown in **Figure-3** for control (room air) and OIR mice using the five-day 75% oxygen treatment model at ages P21, P28 and P42. This confirmed that our model was working as expected. By age P21, regions of INL thinning have resulted due to the loss of bipolar cells during the vascular ablation phase in the model. By P21 neovascular growth has restored oxygen to the central inner retinal zones that were ablated. OIR retinas have central regions of INL (inner nuclear layer) thinning of varied severity. These included complete loss of the INL and ganglion cell layer, as well as regions of transition between zones of extensive bipolar cell loss (vascular ablation regions) and zones of less severe cell loss. In these experiments we did not see any significant loss of photoreceptor cells in the OIR mice compared to room air controls. The ONL (outer nuclear layer) of OIR retinas appeared to maintain the same thickness as their normal air counterparts. As expected the OIR treatment mostly impacted the survival of inner retinal neurons that died during the period of hypoxia.

Figure 3. Erosion of the INL and GCL in the central retina of the OIR mouse model.
Light microscopy sections of mouse retinas are shown for normal control (room air) and oxygen-treated mice at the same three ages used for focal-ERG recordings, illustrating that ablation of the retinal vasculature during the 75% oxygen treatment results in a varied amount of bipolar cell loss by age P21. Some examples of thinning of the inner nuclear layer and transition to regions of near normal looking retina are shown at ages P21, P28 and P42. Regions of bipolar cell loss are evident (white arrows). Some retinal regions are severely affected to the point where ganglion cell density is also decreased (black arrow). The peripheral retina is generally spared. (RPE - Retinal pigment epithelium; IS/OS – Inner and Outer Segments; ONL – outer Nuclear Layer; INL – Inner Nuclear Layer; GCL – Ganglion cell layer)

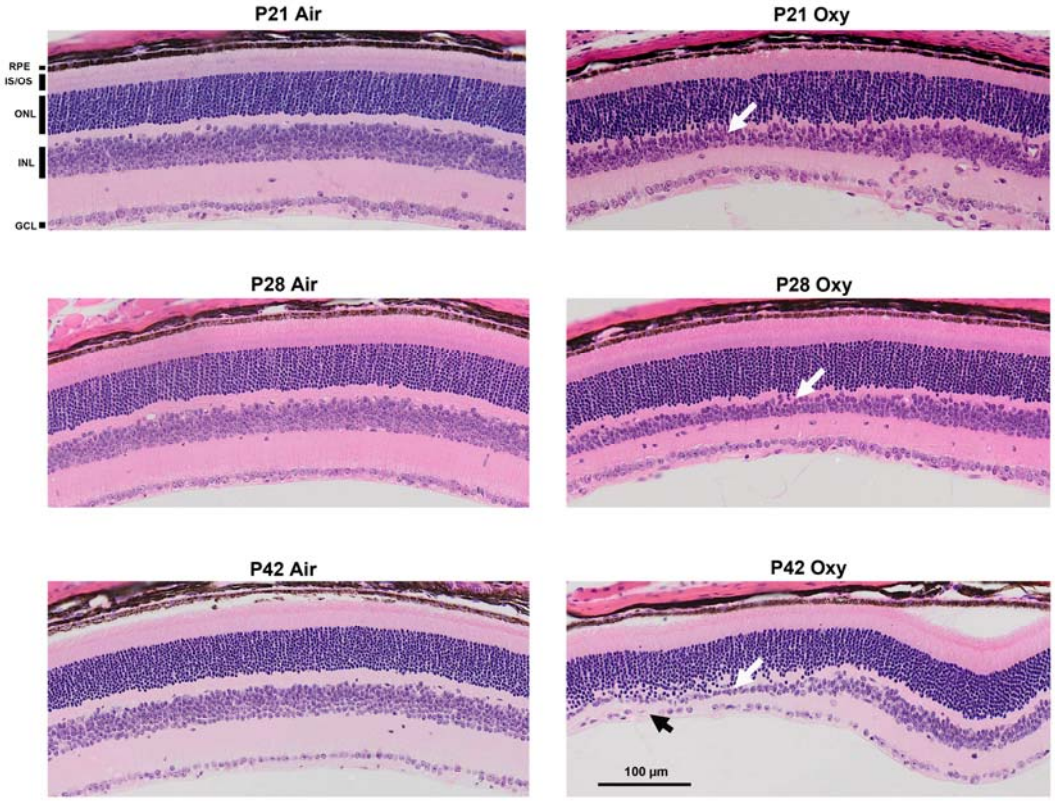

Focal ERG B-wave intensity in areas of different INL thickness

To demonstrate that we can use focal-ERG testing of different small areas within the same retina without excessive interference from more peripheral retina areas, we used SD-OCT to map zones of different INL thickness un an OIR retina to select discrete targets for stimulation and recording of the ERG. The loss of bipolar cells and thus INL thinning was expected to be more severe in central regions of vascular ablation compared to central

regions that do not experience vessel ablation. This was confirmed by imaging the same retina on two different days using fluorescein angiography guided SD-OCT. Live image guided SD-OCT shows the retinal layers in an central zone that was ablated of retinal vessels as well as an adjacent region that was not ablated at age P18. (See Figure 4A,C) By age P23, after revascularization, the formerly ablated zone had a relatively thinner INL (Figure 4B,D).

Figure 4. Relation of central avascular zones to INL thinning. INL thinning is more severe in central avascular zones. SD-OCT imaging of the same OIR retina at ages P18 and P23. SD-OCT scans were taken, in the direction of the red arrows, within the period of aggressive neovascularization at age P18 and at age P23 after resolution of vascular regrowth. **A)** At age P18, a linear OCT scan location was selected using fluorescein-angiography guided-imaging to compare an avascular zone (start of scan) transition into a vascular zone. Some fluorescein image image-blur was apparent, from imaging through perfused vessels that are still present on the lens posterior. **B)** The same retina subjected to a repeated OCT linear scan at age P23 after revascularization of the central retina avascular zones. **C)** The OCT image at age P18, corresponding to the location shown above in panel A. **D)** OCT image at age P23, corresponding to the location shown above in panel B.

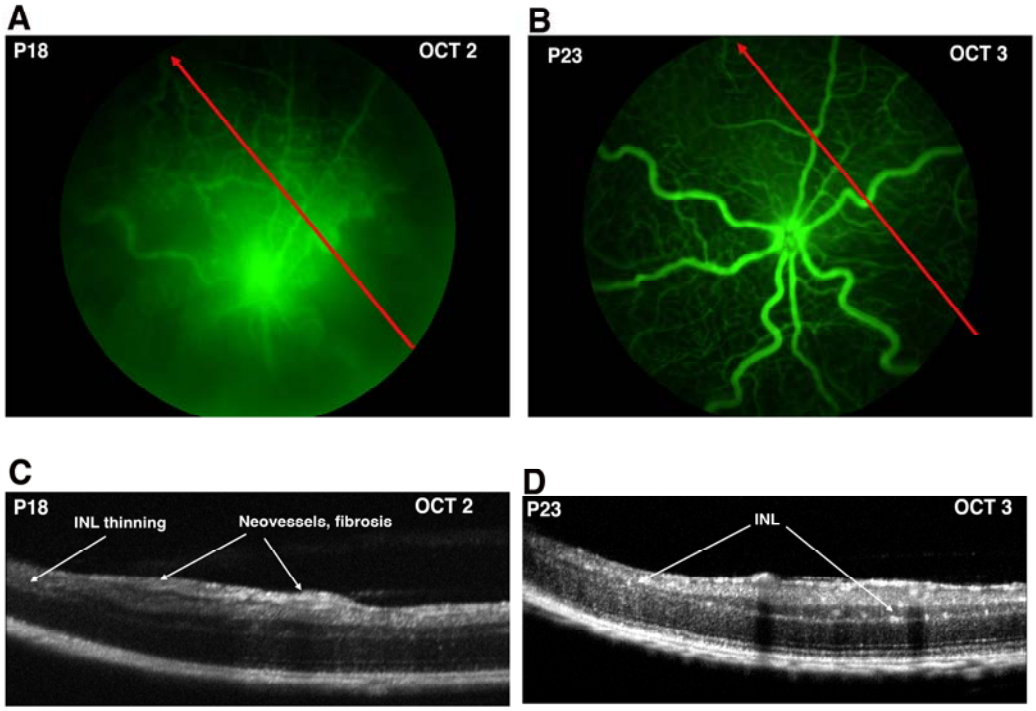

211 This same retina was also mapped in more detail at age P23 with several SD-OCT scans to
212 locate central zones with relatively thinner or thicker INL. (Figure 5A) Based on this
213 information the same retina was tested by focal-ERG at age P37 to compare two zones of
214 relatively thinner INL to two zones with relatively thicker INL at the same distance from the
215 disc (Figure 5B).
216

Figure 5. Local variations in B-wave amplitude detected relative to surviving INL thickness.
The same retina shown in Figure-3 was mapped by SD-OCT to identify locations of relatively thinner and thicker INL for functional comparison. **A)** To establish that the focal-ERG stimulation can compare B-wave intensity in small adjacent regions with different amounts of bipolar cell loss after oxygen-induced retinopathy (OIR), an OIR retina P23) was first mapped using SD-OCT with linear scans (1.4 mm long). Scans were placed precisely during live imaging with fluorescein angiography. Extensive bipolar cell loss was visible in all OCT scans of the central retina. SD-OCT scan directions are indicated by lines with arrows and the line colors (red, green, blue) correspond to the OCT images in the same colored boxes to the right. The start of each scan corresponds to the left-side of the OCT image. An example of a relatively thinner INL layer with more extensive bipolar cell loss is indicated (white arrow) in the topmost scan (red).
B) In a follow up session (age P37) four small circular areas of equal distance from the optic disc were targeted for focal-ERG. Bright flashes were used to elicit a mixed rod-cone response using circular projected light flashes of actual size shown by the numbered red circles (0.27 mm diameter). Targets 1 and 2 were selected to represent regions of relatively thinner INL compared to target regions 3 and 4. **C)** Regions were focal-ERG tested in the relative temporal order 1 to 4. Both regions of relatively thinner and similar INL thickness (targets 1 and 2) had a smaller B-wave amplitude than the relatively thicker regions (targets 3 and 4).

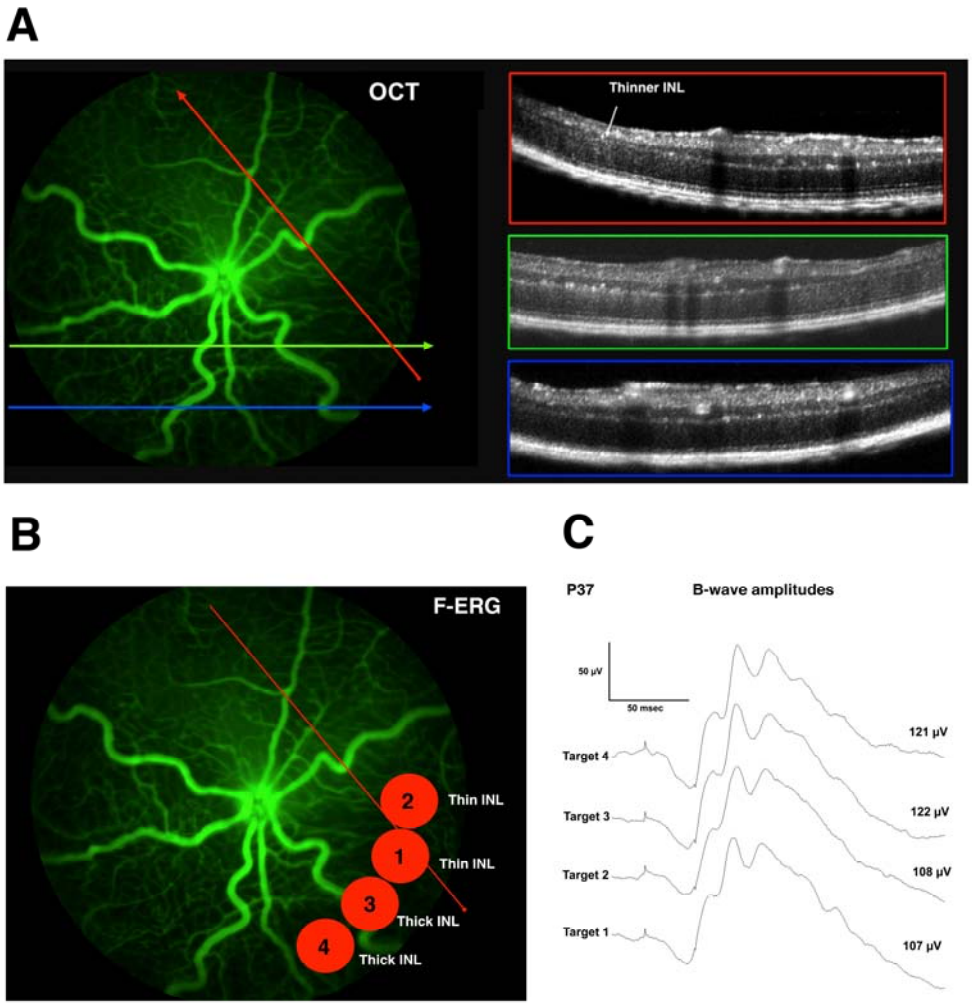

Focal-ERG recordings were made during the bright flash stimulation (mixed rod-cone response) and are shown in Figure 5C. Two target regions with relatively thin inner retinas (labeled 1 and 2) were tested, followed by testing of two regions with relatively thicker inner retinas (labeled 3 and 4). Targets with thinner inner retinas had similar B-wave intensities, which were less than the intensities derived from targets with thicker inner retinas. With the ability to detect differences in B-Wave intensity between regions of different INL thickness that were essentially adjacent, we concluded that any interference at a distance would not preclude focal-erg testing of zones that are much further apart, in completely different retinal quadrants.

Local recovery of B-wave in central affected regions of the OIR mouse retina.

To follow functional changes over time in the same retina we followed an OIR retina and a normal retina over a period of three weeks using image-guided focal-ERG. The same areas of the same retinas were compared longitudinally starting at age P21, after revascularization of the central ablated zone that occurs in this model. The fluorescein angiograms of the retinas followed over three weeks are shown at age P42. (**Figure 6**). This mouse strain had endogenous expression of the YFP protein in a subset of retinal ganglion cells that are also visible prior to injection of fluorescein. Figure 6 shows imaging of the retina through the Focal-ERG's lens using a fluorescein filter set just after the final ERG testing at age P42. The typical appearance of the normal retinal vasculature was seen in the control retina (Figure 6A). In contrast the OIR retina displayed the torturous retinal vasculature that is familiar and characteristic of retinas that have undergone vascular ablation and neovascular regrowth (Figure 6B).

243

Fig 6. Post-ERG Imaging: Fluorescein Angiography and Ganglion Cells (YFP). A) Normal room-air control retina, age P42. In this strain a subset of ganglion cells are also visible (red arrows) from endogenous yellow fluorescent protein using the standard fluorescein filters. Images were captured using the Micron-III's main light through the focal-ERG lens, immediately after collecting focal-ERG data. **B)** Note the torturous vessel morphology in the OIR retina after neovascularization, age P42.

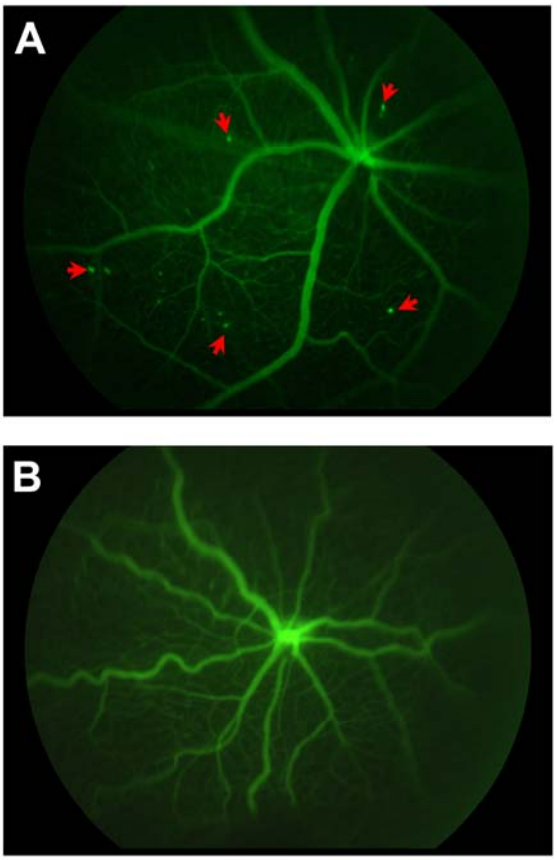

244

245

246

247 Four zones were tested, targeting small circular areas adjacent, but not on, the optic disc.
248 Targets were placed superior, inferior, nasal and temporal around the disc. This targeting
249 process facilitated the testing of the same areas at all three ages for each retina: P21, P28
250 and P42. Focal-ERG traces from the four locations of a normal room air (control) retina and
251 an OIR damaged retina are shown are shown in **Figure-7**.

252

Just after revascularization at P21, a very week B-wave (average 21.9 mV) was seen in all four tested zones of the OIR damaged retina. In comparison, the focal-ERG B-wave amplitudes of a normal retina at age P21 were 10-fold larger (t-test, P<0.0001). See **Table-1**. The normal retina focal-ERG B-wave traces also displayed familiar oscillatory potentials as normally seen with full-field ERG. (**Figure-7**) The weak focal-ERG B-waves of the OIR retina did not display oscillatory potentials at age P21. In contrast to the different B-wave amplitudes between normal and OIR retinas, the photoreceptor-derived A-wave amplitudes were not significantly different between the control and OIR damaged retinas. (Table 1).

Table 1: Focal ERG Average A-wave and B-wave Amplitudes (N=4 locations).

	A-Wave (μV)			B-Wave (μV)		
	P21	P28	P42	P21	P28	P42
Normal Air	-24.5 ± 9.2	-26.0 ± 6.9	-20.1 ± 4.9	221.7 ± 37.2	232.2 ± 27.9	195.6 ± 29.2
OIR	-31.3 ± 7.7	-22.3 ± 5.2	-16.6 ± 4.5	21.9 ± 16.4	40.4 ± 13.7	80.9 ± 37.4
P-value T-test	0.15	0.21	0.16	<0.0001	<0.0001	<0.005

Continuing to compare the focal ERG amplitudes at ages P28 and P42, there was a visible recovery of the B-wave amplitude in the OIR central retinal zones over a three-week span. (**Figure-7**). By age P42 the B-wave amplitudes at each zone tested also began to develop characteristic oscillatory potentials characteristic of retinas with interconnected inner retinal neurons. The local improvement in average focal-ERG B-wave amplitude by age P42 was substantial, about 4-fold greater than that seen at age P21. However, this recovered B-wave amplitude was only 41% of the average B-wave amplitude of an age matched normal retina. In contrast to the lost and recovery of the central retina derived B-wave response, the focal-ERG A-wave amplitudes were not different between the OIR and normal retinas at any of the ages tested.

Figure 7) Partial recovery of the B-wave in the OIR damaged neural retina.
Focal-ERG traces of the combined rod-cone response were obtained using bright flashes of the same four locations in of the same retinas, followed at three different ages: P21, P28 and P42. The control and OIR retinas were tested in the same sessions on the same day. ERG traces from the four locations around the central retina are shown: superior, inferior, nasal and peripheral (relative to the disc). All four locations in the normal retina displayed a normal looking ERG pattern with A-wave, B-wave and oscillatory potentials. In the OIR damaged retina, at P21 the A-wave could be detected with very little B-wave response. Longitudinal analysis of the same retina areas repeated at ages P28 and P42 revealed a gradual appearance and improvement of the B-wave amplitude in the OIR damaged retina, including some oscillatory potentials.

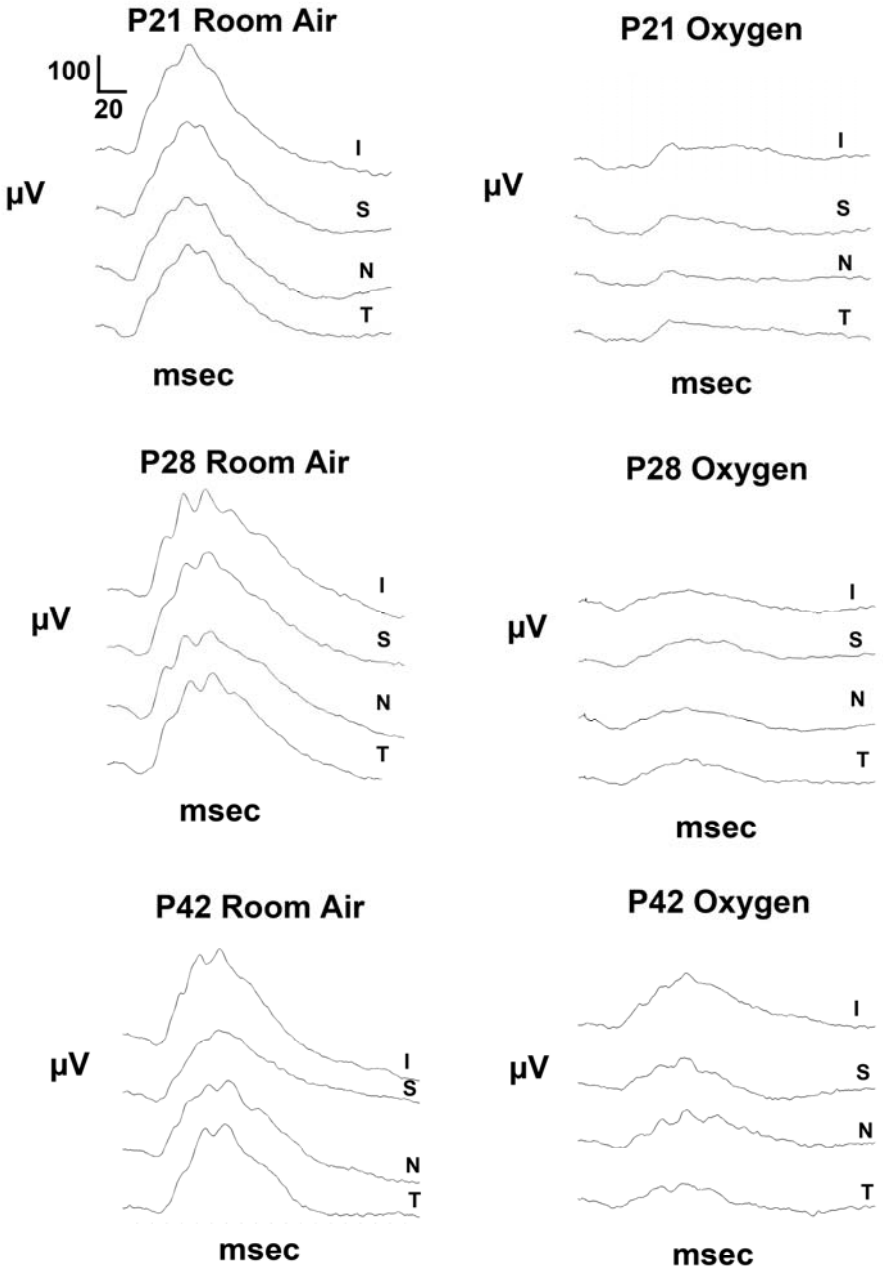

DISCUSSION

The mouse OIR model is useful to produce ischemic retinal areas *in vivo*, which results in neovascular regrowth when the mice are returned to a normal air environment. As such, the model is useful to study the pathophysiology of inner retinal neuron loss during ischemia, as well as the regulation of subsequent neovascular growth [3, 11]. For our investigation here, we focused on the phase subsequent to neovascularization to look for evidence of any local recovery of inner retinal function. With focal-ERG, we limited the light-flash stimulation to extremely small retinal zones that were just larger than the disc. This enabled us to test the function of the inner retina in the OIR-damaged area, based on the ERG B-wave response that is dominated by bipolar cell depolarization [14]. While other human, rat and mouse studies provide good evidence that there is an overall average recovery of post-photoreceptor function [6, 8, 10], our use of focal-ERG stimulation to longitudinally monitor the same small retinal areas of an OIR retina over a period of several weeks suggest that recovery can take place in regions that have suffered OIR induced damage.

In the normal mouse retina, the focal-ERG A- and B-wave amplitudes are generally less than when stimulating the entire retinal area (full-field ERG), but the ERG features are familiar and similar in pattern to that of the full-field ERG. A-wave, B-wave and oscillatory potentials were clearly derived and reproducible using the time averaging of twenty traces per area tested. Quite small retinal areas (0.27 mm diameter) were tested close to the disc, to ensure the targeting of central retinal regions that experienced vascular ablation. These same regions experienced bipolar cell loss during the ischemia phase of the model that resulted after 75% oxygen-treated mice were returned to room air (21% oxygen). It is established by other laboratories, and our own, that aggressive neovascular growth returns the inner retina's blood supply by age P21 [3, 12, 13]. We wanted to investigate the functional status of these central OIR damaged retinal zones from age P21 onward. With the substantial death of bipolar cells during the ischemic phase, would the OIR damaged retina areas function at age P21, compared to the normal? Subsequently, would the function of these damaged zones remain the same or recovery over the next several weeks?

From histology and OCT we concluded that most of the cell death in the OIR damaged central retinal zones involved the inner retina, seen as a reduction in the INL

thickness. In contrast the ONL remained a normal thickness (10-12 photoreceptor nuclei) even in regions where almost all bipolar neurons were lost (Figure 3). This reflects the fact that photoreceptor cell inner-segments, and their oxygen-demanding mitochondria, are adjacent to the RPE/choroid and the choroid's blood supply. Thus, photoreceptors cells are less reliant on the three vascular beds of the inner retina, which were ablated during the 75% oxygen treatment phase. This was consistent with the near normal A-wave amplitude seen in OIR damaged central retinal zones when compared to room-air control central retinal zones. Photoreceptors remained normal in number and functionally mature enough to respond to light stimulation and generate a negative A-wave of similar amplitude to the normal retina.

Consistent with the loss of bipolar cells, the central retinal B-wave amplitudes were substantially reduced and abnormal in their pattern at age P21 in the OIR retina. At P21 the B-wave was essentially decimated. Furthermore, longitudinal follow-up of the same local central zones at ages P28 and P42 revealed a progressive and significant recovery of the B-wave amplitude. The recovery of familiar oscillatory potentials superimposed on the B-wave was also apparent in the OIR focal-ERG by age P42.

Our results suggest that there was a non-functional inner retina at age P21 immediately after the loss of bipolar cells and that these damaged central retinal zones demonstrated a local recovery of inner-retinal function by establishing their functionality. This was seen in the local recovery of the B-wave amplitude. However, the recovered B-wave amplitude at age P42 remained less than seen in a normal retina with full compliant bipolar cells. One implication of these results is that any surviving inner retina neurons do have the ability to recover function over time. This might involve physical reorganization [9](i.e. synaptogenesis) and also a metabolic recovery from pan-retinal changes in energetics and ion regulation[15].

Regarding human conditions involving ischemic retinal neuron loss, such as ROP, our results suggest that any treatments that improve bipolar cell survival would result in an overall improvement in the final retinal function. Thus, such treatments, even if not perfect, would be worthwhile. Finally, the use of focal-ERG combined with imaging technologies, such as angiography, and SD-OCT provided us with the ability to explore retinal function in more detail than we could previously. Multiple combined imaging and focal-ERG testing, with image guided targeting, could provide an expanded range of non-invasive diagnostic

tools for more detailed understanding of retinal pathologies in the human eye *in vivo*.

Acknowledgments

Research Support: Vision Research ROPARD Foundation, (Virginia and Clarence Clohset estate) to KPM and KD. Oakland University Center for Biomedical Research to KPM. Special Trustees of Moorsfields Eye Hospital, National Institute of Health Biomedical Research Center at Moorsfields Eye Hospital, UCL Institute of Ophthamalology, TFC Frost Trust, HCA International, and Moorsfields Surgeons Association for visiting fellowship to SCW. Authors acknowledge Jennifer Felisky, OU student, for assistance in manuscript submission and reviewing.

References

1. Gole GA, Browning J, Elts SM. The mouse model of oxygen-induced retinopathy: A suitable animal model for angiogenesis research. Doc Ophthalmol. 1990; **74**:163-9.
2. Ricci B. Oxygen-induced retinopathy in the rat model. Doc Ophthalmol. 1990; **74**:171-7.
3. Smith LE, Wesolowski E, McLellan A, et al. Oxygen-induced retinopathy in the mouse. Invest Ophthalmol Vis Sci. 1994; **35**:101-11.
4. Krohne TU, Westenskow PD, Kurihara T, et al. Generation of retinal pigment epithelial cells from small molecules and oct4-reprogrammed human induced pluripotent stem cells. Paediatr Int Child Health. 2012; **1**:96-109.
5. Fulton AB, Hansen RM, Moskowitz A, Akula JD. The neurovascular retina in retinopathy of prematurity. 2009; **28**:452-82.
6. Fulton AB, Hansen RM, Moskowitz A. The cone electroretinogram in retinopathy of prematurity. 2008; **49**:814-9.
7. Akula JD, Hansen RM, Martinez-Perez ME, Fulton AB. Rod photoreceptor function predicts blood vessel abnormality in retinopathy of prematurity. 2007; **48**:4351-9.
8. Fulton AB, Akula JD, Mocko JA, et al. Retinal degenerative and hypoxic ischemic disease. 2009; **118**:55-61.
9. Harris ME, Moskowitz A, Fulton AB, Hansen RM. Long-term effects of retinopathy of prematurity (rop) on rod and rod-driven function. 2011; **122**:19-27.
10. Nakamura S, Imai S, Ogishima H, et al. Morphological and functional changes in the retina after chronic oxygen-induced retinopathy. PLoS One. 2012; **7**:e32167.
11. Pierce EA, Avery RL, Foley ED, Aiello LP, Smith LE. Vascular endothelial growth factor/vascular permeability factor expression in a mouse model of retinal neovascularization. Proc Natl Acad Sci U S A. 1995; **92**:905-9.
12. Wang L, Shi P, Xu Z, et al. Up-regulation of vegf by retinoic acid during hyperoxia prevents retinal neovascularization and retinopathy. Invest Ophthalmol Vis Sci. 2014; **55**:4276-87.

13. Tokunaga CC, Mitton KP, Dailey W, et al. Effect of anti-vegf treatment on developing retina following oxygen-induced retinopathy. Invest Ophthalmol Vis Sci. 2014; **55**:1884-1892.
14. Saszik SM, Robson JG, Frishman LJ. The scotopic threshold response of the dark-adapted electroretinogram of the mouse. J Physiol. 2002; **543**:899-916.
15. Berkowitz BA, Roberts R. Evidence for a critical role of panretinal pathophysiology in experimental rop. 2010; **120**:13-24.